(Received 3 December 2025, Accepted 20 January 2026, Scheduled 3 February 2026)

Adaptive Model-Free Sliding Mode Fault-Tolerant Speed-Current Control for Permanent Magnet Synchronous Motor under Extreme Operating Conditions with Parameters Mismatch

Junqin Liu[1,*], Haicheng Zhong[1], Zhentong Wang[1], Xinchun Jiang[2], Yilin Chen[3], Daoyi Gu[4], Kaihui Zhao[2], Xiangfei Li[2], and Lin Liu[1]

[1] *College of Electrical and Information Engineering, Changsha University of Science and Technology, Changsha 410114, China*
[2] *College of Transportation and Electrical Engineering, Hunan University of Technology, Zhuzhou 412007, China*
[3] *State Grid Hunan Province Electric Power Co., Ltd., Xiangxi Power Supply Branch, Jishou 416000, China*
[4] *State Grid Hunan Province Electric Power Co., Ltd., Zhangjiajie Power Supply Branch, Zhangjiajie 427000, China*

ABSTRACT: To address the limitations of Permanent Magnet Synchronous Motor (PMSM) speed-current closed-loop systems, including control performance degradation due to PI controller integral saturation and insufficient convergence in traditional model predictive current control (MPCC) while simultaneously reducing the computational load in the control system, this study combines model-free control theory with higher-order sliding mode methods and proposes an adaptive nonsingular terminal model-free sliding mode composite control strategy (ANTMFSMC) that considers parameter mismatch. First, based on the mathematical model of PMSM and the model-free theory for nonlinear systems, a speed-current loop control model is established. By combining the nonsingular terminal sliding mode with adaptive sliding mode reaching law, a speed-current loop ANTMFSMC controller is designed, and an improved exponential sliding mode disturbance observer (INTSMDO) is constructed to estimate the unknown components of unmodeled dynamics and parameter uncertainties in the system. These estimates are then introduced as a feedforward compensation into the ANTMFSMC controller to form a complete composite control architecture. Finally, through simulations and experimental comparisons with traditional PI control and the traditional nonsingular terminal model-free sliding mode control based on sliding mode disturbance observer method (NTMFSMC-SMDO), the results show that the proposed strategy effectively suppresses d-q axis current and voltage ripple, significantly improves the convergence speed and anti-disturbance capability of the system, and demonstrates good engineering application value.

1. INTRODUCTION

With the rapid evolution of modern electric drive technologies, permanent magnet synchronous motors (PMSMs) have been extensively employed in transportation systems, process and manufacturing industries, aerospace platforms, and residential applications [1]. These applications require current and torque responses with high bandwidth, low ripple, and strong robustness. In the widely adopted field-oriented control (FOC) scheme, three-phase stator currents are transformed into a rotating reference frame via the Clarke-Park transformation, and d-q axis current loops are independently regulated to achieve the decoupled control of the stator flux and electromagnetic torque. Accordingly, the dynamic and steady-state performances of the entire drive system are predominantly determined by the behavior of inner current control loops [2].

In the conventional PMSM control framework based on field-oriented control (FOC) with dual proportional-integral (PI) current regulators, the d- and q-axis currents are independently regulated using PI controllers to track their references, whereas feedforward compensation and cross-coupling decoupling are introduced to enhance the transient response [3]. However, this approach relies heavily on the accuracy of the motor's equivalent model and fails to guarantee a high-precision current-tracking performance under varying operating conditions [4]. To mitigate the performance degradation of current loops caused by parameter variations associated with temperature rise, magnetic saturation, and frequency-dependent effects, numerous studies have investigated online parameter identification and self-tuning PI schemes. Representative techniques include model-based closed-loop PID/PI autotuning and optimization-based parameter search methods, which adapt controller gains to different operating conditions [5]. Nevertheless, parameter-identification-based or self-tuning PI solutions still exhibit performance limitations when being faced with wide operating ranges, stringent harmonic-suppression requirements, and strong parameter uncertainties [16]. In recent years, model predictive current control (MPCC), which exploits the discrete-time mathematical model of a motor, has emerged as an important research direction for PMSM current regulation. MPCC methods are generally categorized into finite control set (FCS-MPC) and

* Corresponding author: Junqin Liu (ljq2321925777@163.com).

continuous control set (CCS-MPC) approaches, among which the performance of FCS-MPC is highly sensitive to the model accuracy [6]. Although the MPCC offers notable advantages of transient performance and control flexibility, it suffers from a high computational burden and sensitivity to sampling and computation delays. With the increasing computational capability and the rise of data-driven techniques, recent studies have explored the application of artificial intelligence algorithms to PMSM current and speed control [7]. For instance, comparative analyses of deep reinforcement learning methods (e.g., DQN, PPO, and A2C) have demonstrated that intelligent controllers can potentially outperform conventional PI and MPCC schemes in scenarios characterized by strong nonlinearity or rapidly varying operating conditions [8]. These approaches rely less on accurate mathematical models and can adapt to different machines and operating environments through learning. However, significant challenges remain in terms of interpretability, stability guarantees, and engineering applicability, including data acquisition for training and real-time computational requirements [9].

To achieve high-performance PMSM control while retaining interpretability and ensuring rigorous stability guarantees, this study addresses the nonlinear and strongly coupled characteristics of PMSMs by integrating sliding mode control (SMC) with model-free control (MFC) theory [10]. Accordingly, an adaptive terminal model-free sliding mode control scheme was developed for the PMSM speed-current regulation structure. As a distinctive nonlinear control methodology, SMC has attracted extensive attention because of its inherent switching characteristics and strong robustness against disturbances and parameter uncertainties, making it an important focal point in modern control theory and engineering applications [11]. Unlike conventional linear control techniques, SMC does not rely on a fixed control architecture; instead, it actively modifies the control action based on the real-time system state, guiding the system trajectory along a predefined sliding manifold that is inherently insensitive to external disturbances and state variations [12]. Consequently, SMC offers advantages such as strong robustness, reduced sensitivity to parameter deviation, and ease of implementation [13]. Its dynamic adaptability allows the control mechanism to conform better to rapidly varying operating conditions while effectively handling uncertainties, thereby ensuring stable and optimized performance in complex dynamic environments [14]. Model-free control (MFC) has emerged as an effective approach to mitigate system-parameter perturbations and has increasingly been applied in PMSM drive systems [15]. In contrast to traditional model-based control strategies that rely on accurate system representations, MFC adaptively update the control law through real-time interaction between system inputs and outputs, substantially reducing their dependence on precise model information. By eliminating the strict structural assumptions of the plant model, the MFC maintains satisfactory control accuracy and dynamic response even under parameter uncertainties and model mismatches. Owing to their data-driven nature, MFC demonstrates notable advantages in motor-driven scenarios characterized by complex dynamics, strong coupling, and nonlinear behavior. Given the intricate structure and frequent parameter variations inherent in PMSM systems, traditional model-based strategies often struggle to balance the performance and robustness, whereas MFC exhibits strong adaptability and disturbance resilience, making them highly suitable for such applications [17].

To enhance the control performance of the PMSM speed-current closed-loop system while reducing the computational burden and ensuring a model-independent control mechanism, this study integrates the model-free control theory with a high-order sliding mode strategy and proposes an adaptive terminal model-free sliding mode fault-tolerant control algorithm for PMSM drives. The proposed approach achieves inherent robustness without relying on an explicit motor model and ensures fast dynamic regulation of both speed and current loops. The simulated and experimental results demonstrate that the method effectively suppresses d-q axis current and voltage ripples, significantly improves convergence speed and disturbance rejection capability, and exhibits strong potential for practical engineering applications.

2. ANALYSIS OF MATHEMATICAL MODEL FOR PMSM

Ignoring all losses, the stator voltage equations of the PMSM in the d-q coordinate frame are given as [15]:

$$\begin{cases} u_d = R_s i_d + L_d \frac{di_d}{dt} - \omega_e L_q i_q \\ u_q = R_s i_q + L_q \frac{di_q}{dt} + \omega_e \left(L_d i_d + \psi_f\right) \end{cases} \tag{1}$$

where i_d and i_q represent the stator d-q axis current components; u_d and u_q represent the stator d-q axis voltage components; L_d and L_q are the stator d-q axis inductances; ψ_f is the permanent magnet flux linkage; R_s is the stator resistance; ω_e is the electrical angular velocity.

The electromagnetic torque and mechanical motion equations of the motor are given by:

$$\begin{cases} T_e = \frac{3}{2} n_p \left[\psi_f + (L_d - L_q) i_d\right] i_q \\ \frac{J}{n_p} \cdot \dot{\omega}_e = T_e - T_L - B\omega_m \end{cases} \tag{2}$$

where T_e is the electromagnetic torque, n_p the number of pole pairs, ψ_f the flux linkage, J the moment of inertia, T_L the load torque, B the viscous friction coefficient, and ω_m the mechanical angular velocity.

Under high-speed operations, parameter variations and external disturbances are inevitable in PMSM. Variations in the magnitude and spatial angle of the permanent-magnet flux linkage may give rise to demagnetization faults. The amplitude variation of the PMSM electromagnetic parameters can be described by

$$\begin{cases} R_{so} = R_s + \Delta R_s \\ L_{do} = L_d + \Delta L_d \\ L_{qo} = L_q + \Delta L_q \\ \psi_{fo} = \psi_f + \Delta \psi_f \end{cases} \tag{3}$$

where R_{so}, L_{do}, L_{qo}, and ψ_{fo} denote the actual values of the PMSM electromagnetic parameters in the presence of parameter mismatch; ΔR_s denotes the perturbation of the stator phase resistance; ΔL_d and ΔL_q represent the perturbations of the d-

and q-axis stator inductances, respectively; $\Delta\psi_f$ denotes the perturbation of the rotor flux linkage.

From Eq. (3), taking parameter mismatches into account, Eq. (1) can be expressed as

$$\begin{cases} u_d = R_{so}i_d + L_{do}\frac{di_d}{dt} - \omega_e L_{qo} i_q + \Delta u_d \\ u_q = R_{so}i_q + L_{qo}\frac{di_q}{dt} + \omega_e \left(L_{do}i_d + \psi_{fo}\right) + \Delta u_q \end{cases} \tag{4}$$

where Δu_d is the change in the d-axis voltage caused by parameter perturbations, and Δu_q is the change in the q-axis voltage caused by parameter perturbations.

From Eq. (2), the electromagnetic torque equation of the PMSM can be expressed as

$$T_e = \frac{3}{2} n_p \left[\psi_{fo} + (L_{do} - L_{qo}) i_d\right] i_q + \Delta T_e \tag{5}$$

where ΔT_e is the change in electromagnetic torque.

From Eq. (2) and Eq. (5), the state equation of the PMSM speed loop is given by:

$$\begin{aligned} \dot{\omega}_e &= \frac{\frac{3}{2} n_p \psi_e i_q - T_L - \Delta T_e + \Delta T_L}{J} - \frac{B\omega_m}{J} + \delta_d \\ &= \frac{3n_p^2}{2J}\psi_e i_q + F_\omega \end{aligned} \tag{6}$$

where $\psi_e = \psi_{fo} + (L_{do} - L_{qo}) i_d$; δ_d denotes the unmodeled dynamics of the system; F_ω represents the bounded total disturbance caused by parameter changes.

3. ESTABLISHMENT OF SPEED-CURRENT LOOP CONTROL MODEL BASED ON MODEL-FREE CONTROL THEORY FOR PMSM

3.1. Model-Free Control Theory for Nonlinear System

For a nonlinear, single-input single-output (SISO) system, the model can be represented as [1]

$$\begin{cases} y^{(v)} = g(x) + \varphi u \\ y = x \end{cases} \tag{7}$$

where y and u are the output and input of the control system, respectively; $x \in R$ represents the state variables of the system; $\varphi \in R$ is a constant gain to be designed for the system.

$$g(x) = F \tag{8}$$

where F represents an unknown disturbance term in the system.

By combining Eq. (7) and Eq. (8), the new ultra-local model can be obtained as

$$\dot{x} = \varphi u + F \tag{9}$$

3.2. Establishment of Model-Free Mathematical Model for Speed-Current Loop of PMSM

The state equation for the d-q axis current loop of the system under parameter perturbations can be expressed as

$$\begin{cases} \frac{di_d}{dt} = \frac{1}{L_{do}}u_d - \frac{R_{so}}{L_{do}}i_d + \omega_e \frac{L_{qo}}{L_{do}} i_q + f_d \\ \frac{di_q}{dt} = \frac{1}{L_{qo}}u_q - \frac{R_{so}}{L_{qo}}i_q + \omega_e \frac{L_{do}}{L_{qo}} i_d - \frac{\omega_e}{L_q}\psi_e + f_q \end{cases} \tag{10}$$

where f_d and f_q denote the uncertain disturbance terms of the d-q axis current loops under parameter perturbations.

The PMSM system adopts the $i_d = 0$ control strategy, where $L_d = L_q = L_s$. Based on Eq. (6) and Eq. (10), the model-free mathematical representation of the PMSM speed-current loop can be derived as

$$\begin{cases} \frac{di_d}{dt} = \frac{1}{L_{do}}u_d - \frac{R_{so}}{L_{do}}i_d + \omega_e \frac{L_{qo}}{L_{do}} i_q + f_d = \varphi_d u_d + F_d \\ \frac{di_q}{dt} = \frac{1}{L_{qo}}u_q - \frac{R_{so}}{L_{qo}}i_q + \omega_e \frac{L_{do}}{L_{qo}} i_d - \frac{\omega_e}{L_q}\psi_e + f_q \\ \quad = \varphi_q u_q + F_q \\ \frac{d\omega_e}{dt} = \frac{3n_p^2}{2J}\psi_e i_q + F_\omega = \varphi_\omega i_q + F_\omega \end{cases} \tag{11}$$

where φ_d, φ_q, φ_ω are the parameters to be designed; F_d is the total disturbance in the motor's d-axis current loop; F_q is the total disturbance of the q-axis current loop; F_ω is the total disturbance of the motor's speed outer loop.

From Eq. (11), Eq. (12) can be expressed as

$$\dot{x}_i = \varphi_i u_i + F_i \tag{12}$$

where φ_i and $F_i (i = \{d, q, \omega\})$, $\varphi_i = \{\varphi_d, \varphi_q, \varphi_\omega\}$, $F_i = \{F_d, F_q, F_\omega\}$; $u_i = \{u_d, u_q, i_q\}$; $x_i = \{i_d, i_q, \omega_e\}$.

4. DESIGN OF ANTMFSMC-INTSMDO COMPOSITE CONTROLLER FOR SPEED-CURRENT LOOP

4.1. Design of ANTMFSMC Controller

The expression for the speed-current model-free sliding mode controller can be obtained from Eq. (12) as

$$u_i^* = \frac{1}{\varphi_i} \cdot \left(\dot{x}_i^* - F_i + \rho_i\right) \tag{13}$$

where $(i = i_d, i_q, \omega_e)$, x_i^* represents the reference input value for the speed-current loop; u_i^* denotes the output value of the speed-current loop; ρ_i defines the control law of the controller.

By combining Eq. (12) and Eq. (13), we obtain $\rho_i = -(\dot{x}_i^* - \dot{x}_i)$. Defining the errors $\dot{e}_i = -\rho_i$ and designing $e_{1i} = \int e_i$, $e_{2i} = e_i$. Then, the nonsingular terminal sliding surface [16] can be designed as

$$s = e_{1i} + \beta_i e_{2i}^a \tag{14}$$

where $\beta_i > 0 (i = i_d, i_q, \omega_e)$, $a = 5/3$.

By taking the derivative of Eq. (14), Eq. (15) can be expressed as

$$\dot{s}_i = \dot{e}_{1i} + \beta_i a e_{2i}^{a-1} \dot{e}_{2i} \tag{15}$$

The adaptive exponential sliding mode reaching law can be selected as

$$\dot{s}_i = \frac{-k_i \mathrm{sgn}(s_i)}{\lambda + (1-\lambda) e_i^{-\alpha|s|}} - \gamma_i s_i \tag{16}$$

where $k_i > 0, \gamma_i > 0 (i = i_d, i_q, \omega_e)$; $\alpha > 0$; $0 < \lambda < 1$.

By combining Eq. (13), Eq. (15), and Eq. (16), the control law ρ_i can be designed as:

$$\rho_i = \frac{e_{2i}^{2-a}}{\beta_i a} + \frac{k_i \mathrm{sgn}(s_i)}{\lambda + (1-\lambda) e_i^{-\alpha|s|}} + \gamma_i s_i \tag{17}$$

Proof 1: To analyze the stability of the controller, the Lyapunov stability function was designed as $V_i = \frac{1}{2} s_i^2$. By differentiating V_i:

$$\begin{aligned}\dot{V}_i &= s_i \cdot \dot{s}_i = s_i \left(e_{2i} + \beta_i a e_{2i}^{a-1} \dot{e}_{2i}\right) \\ &= s_i \beta_i a e_{2i}^{a-1} \left(\tilde{F}_i - \frac{k_i}{\lambda + (1-\lambda) e_i^{-\alpha|s|}} \mathrm{sgn}(s_i) - \gamma_i s_i\right) \\ &\le \beta_i a e_{2i}^{a-1} \left[\left(\left\|\tilde{F}_i\right\| - \frac{k_i}{\lambda + (1-\lambda) e_i^{-\alpha|s|}}\right) \|s_i\| - \gamma_i \|s_i\|^2\right]\end{aligned} \tag{18}$$

where $s_i (i = i_d, i_q, \omega_e)$ represents the sliding mode surface.

When $k_i (\lambda + (1-\lambda) e_i^{-\alpha|s|})^{-1} \ge \|\tilde{F}_i\| + \sigma_i (\sigma_i > 0)$ is satisfied, this implies that $\dot{V}_i \le 0$. Therefore, based on this analysis, it can be concluded that the system error converges to zero within a finite time, ensuring the stability of the designed controller.

4.2. Design of INTSMDO Disturbance Observer

To design an IESMDO (Improved Exponential Sliding Mode Disturbance Observer) for accurate estimation of $F_i (i = i_d, i_q, \omega_e)$, define the variable $x_i = \hat{x}_{1i} - x_{1i}$. By introducing the sliding mode observer control law into Eq. (12), the following expression is obtained:

$$\dot{\hat{x}}_i = \varphi_i u_i + \hat{F}_i + g_i \tag{19}$$

where $\hat{F}_i (i = i_d, i_q, \omega_e)$ is the observed value of the unknown disturbance, $\hat{F}_i = A_i g_i$; $A_i (i = i_d, i_q, \omega_e)$ is the gain of the observer; $g_i (i = i_d, i_q, \omega_e)$ is the control rate of the observer.

By combining Eq. (13) and Eq. (19), the observation error can be derived as $\dot{e}_{1i} = e_{fi} + g_i$, where $\dot{e}_{fi} = A_i \cdot g_i - A_i(t)$, $e_{fi} = F_i - F_i$. The nonsingular terminal sliding surface [16] is defined as $l_i = x_i + \mu_i \dot{x}_i^b$. Differentiating this expression yields

$$\dot{l}_i = \dot{x}_i + \mu_i b \dot{x}_i^{b-1} \ddot{x}_i \tag{20}$$

where $\mu_i > 0 (i = i_d, i_q, \omega_e)$, $b = 5/3$.

Selecting the double power sliding mode reaching law [17]:

$$\dot{l}_i = -f_{1i} |l_i|^{h_1} \mathrm{sgn}(l_i) - f_{2i} |l_i|^{h_2} \mathrm{sgn}(l_i) \tag{21}$$

where $f_{1i} > 0$, $f_{2i} > 0$ $(i = i_d, i_q, \omega_e)$; $0 < h_1 < 1$, $h_2 > 1$.

By combining Eq. (20) and Eq. (21), the control law g_i can be derived as:

$$\begin{aligned}g_i &= m_i + n_i = -\int_0^t \left(\frac{\dot{x}_i^{2-b}}{\mu_i b}\right) d\tau \\ &\quad - \int_0^t \left(f_{1i} |l_i|^{h_1} \mathrm{sgn}(l_i) + f_{2i} |l_i|^{h_2} \mathrm{sgn}(l_i)\right) d\tau\end{aligned} \tag{22}$$

Proof 2: Selecting the following Lyapunov function v_i:

$$v_i = \frac{1}{2} l_i^2 \tag{23}$$

where l_i $(i = i_d, i_q, \omega_e)$ denotes the sliding mode surface.

Differentiating v_i and substituting yields:

$$\dot{v}_i = l_i \dot{l}_i = l_i \cdot \mu_i b \dot{x}_i^{b-1} \left(\ddot{x}_i + \frac{\dot{x}_i^{2-b}}{\mu_i b}\right) \tag{24}$$

From Eq. (22), it is known that $\dot{x}_i = e_{fi} + u_{gi}$. Taking the derivative of this expression yields $\ddot{x}_i = \dot{e}_{fi} + \dot{u}_{gi}$. Substituting this into Eq. (24):

$$\begin{aligned}\dot{v}_i &= l_i \cdot \mu_i b \dot{x}_i^{b-1} \left(-\dot{e}_{fi} \cdot l_i + f_{1i} |l_i|^{h_1+1} + f_{2i} |l_i|^{h_2+1}\right) \\ &\le \mu_i b \dot{x}_i^{b-1} \left(-|\dot{e}_{fi}| \cdot |l_i| + f_{1i} |l_i|^{h_1+1} + f_{2i} |l_i|^{h_2+1}\right)\end{aligned} \tag{25}$$

Assuming $|\dot{e}_{fi}| \le M_i$, $M_i \ge 0$, when $f_{2i} |l_i|^{h_2} \ge |\dot{e}_{fi}|$, the following conclusions can be drawn:

$$\dot{v}_i \le \mu_i b \dot{x}_i^{b-1} \left(f_{1i} |l_i|^{h_1+1}\right) \le \mu_i b \dot{x}_i^{b-1} \left(f_{1i1} v_i^{\frac{h_1+1}{2}}\right) \le 0 \tag{26}$$

when $f_{1i} |l_i|^{h_1} \ge |\dot{e}_{fi}|$, the expression can be obtained:

$$\dot{v}_i \le \mu_i b \dot{x}_i^{b-1} \left(f_{2i} |l_i|^{h_2+1}\right) \le \mu_i b \dot{x}_i^{b-1} \left(f_{2i} v_i^{\frac{h_2+1}{2}}\right) \le 0 \tag{27}$$

In conclusion, when $f_{1i} |l_i|^{h_1} \ge |\dot{e}_{fi}|$, $f_{2i} |l_i|^{h_2} \ge |\dot{e}_{fi}|$, it follows that $\dot{v}_i \le 0$, the system error converges to zero within a finite time. The observer given by Eq. (19) is asymptotically stable, and the system state reaches the sliding mode surface in a finite time.

From Eq. (22), the expression for $\hat{F}_i$ is given by:

$$\begin{aligned}\hat{F}_i &= -A_i \left(\int_0^t \left(\frac{\dot{x}_i^{2-b}}{\mu_i b}\right) d\tau \right. \\ &\quad \left. + \int_0^t \left(f_{1i} |l_i|^{h_1} \mathrm{sgn}(l_i) + f_{2i} |l_i|^{h_2} \mathrm{sgn}(l_i)\right) d\tau\right)\end{aligned} \tag{28}$$

To reduce the chattering problem caused by the traditional sgn(**s**) function, function $\Theta(s)$ is used to further suppress chattering. The sign function is replaced by the following equation:

$$\Theta(s_i, l_i) = \begin{cases} \mathrm{sgn}(s_i, l_i); & |s_i, l_i| \ge \Delta \\ \frac{s_i l_i}{\Delta}; & |s_i, l_i| < \Delta \end{cases} \tag{29}$$

where Δ denotes the boundary thickness. Compared to the sgn function $\mathrm{sgn}(s_i, l_i)$, the saturation function provides a smoother switching process, which helps reduce chattering.

By substituting Eq. (17) and Eq. (28) into Eq. (13), the output u_i^* of the PMSM speed-current loop model-free sliding mode controller can be expressed as:

$$u_i^* = \frac{\begin{array}{c}\dot{x}_i^* + A_i \left(\int_0^t \left(\frac{\dot{x}_i^{2-b}}{\mu_i b}\right) d\tau + \int_0^t \left(f_{1i} |l_i|^{h_1}\right. \right. \\ \left. \left. \mathrm{sgn}(l_i) + f_{2i} |l_i|^{h_2} \mathrm{sgn}(l_i)\right) d\tau\right) + \rho_i\end{array}}{\varphi_i} \tag{30}$$

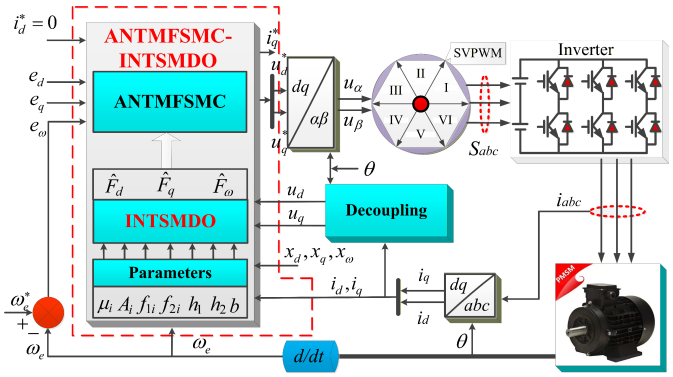

FIGURE 1. Block diagram of the ANTMFSMC-INTSMDO.

5. ANALYSIS OF SIMULATION RESULTS

MATLAB simulation and a semi-physical experimental platform were used to simulate and experimentally validate the ANTMFSMC-INTSMDO control strategy based on the speed-current loop of the PMSM. The performance of the proposed strategy was compared with that of the traditional PI and NTMFSMC-SMDO control methods through both simulated and experimental results. Fig. 1 shows a block diagram of the ANTMFSMC-INTSMDO speed-current loop composite control system. The PMSM parameters are presented in Table 1.

TABLE 1. The parameters of PMSM.

Motor parameters	Value
Permanent magnet flux linkage ψ_f	0.171 Wb
Stator inductance L_s	0.00334 H
Stator resistance R_s	1.9 Ω
Number of pole pairs n_p	4 pairs
Moment of inertia J	0.001469 kg · m^2
Damping coefficient B	0.001 N · m · s/rad

Note 1: NTSMC-SMDO uses a nonsingular terminal sliding mode surface $s = e_{1i} + z_i e_{2i}^a$ and traditional exponential reaching law $\dot{s}_i = -p_i \text{sgn}(s_i) - u_i s_i$, $z_i > 0$, $p_i > 0$, $u_i > 0$ $(i = i_d, i_q, \omega_e)$, $a = 5/3$. Observer SMDO uses a first-order error sliding mode surface $l_i = x_i = \hat{x}_{1i} - x_{1i}$ and traditional exponential reaching law $\dot{l}_i = -r_i \text{sgn}(l_i) - t_i s_i$, $r_i > 0$, $t_i > 0 (i = i_d, i_q, \omega_e)$.

Note 2: The initial load torque was set to $T_L = 5\,\text{N} \cdot \text{m}$, the initial speed set to 1000 r/min, and after $t = 0.3$ s, the speed changes to 2000 r/min. Simultaneously, parameters such as flux linkage, resistance, and inductance are subject to perturbations to verify the disturbance rejection capability of the speed-current loop ANTMFSMC-INTSMDO control strategy. At 0.2 s and 0.5 s, demagnetization faults with amplitude and angle deviations were simulated, where parameters ψ_f and θ_e are set with mismatches within specified ranges. The parameters perturbation conditions are listed in Table 2.

TABLE 2. The perturbation range of parameters.

Parameters	Time	Range
ψ_f/Wb	0.2 s	$0.171 \rightarrow 0.150$
θ_e/rad	0.5 s	$0 \rightarrow \pi/6$
R_s/Ω	0.6 s	$1.9 \rightarrow 3.0$
L_s/mH	0.7 s	$3.34 \rightarrow 4.67$
J/kg · m^2	0.8 s	$1.469 \times 10^{-3} \rightarrow 2.5 \times 10^{-3}$
B/N · m · s/rad	1.0 s	$0.001 \rightarrow 0.004$
T_L/N · m	1.2 s	$5 \rightarrow 8$

5.1. Analysis of Simulation Results for Three Algorithms

The simulation results of the PI, NTMFSMC-SMDO, and ANTMFSMC-INTSMDO methods were compared. Fig. 2(a) shows the speed simulation results. Fig. 2(b) shows the output torque simulation results. Fig. 2(c) and Fig. 2(d) show the d-q axis current simulation results.

Figure 2(a) shows the simulated speed responses under the three control strategies. As illustrated, the PI controller suffers from a pronounced overshoot during speed regulation, which is primarily caused by integral saturation. The NTMFSMC-SMDO approach alleviates this overshoot but requires a longer settling time to reach the reference speed. In comparison, the proposed ANTMFSMC-INTSMDO method achieves rapid and overshoot-free tracking of the speed command, indicating a markedly improved dynamic behavior. When the parameters are perturbed, the enlarged view reveals that ANTMFSMC-INTSMDO maintains a higher disturbance-rejection capability; its speed promptly reconverges and follows the reference more accurately. Moreover, under time-varying external disturbances, this method exhibits the smallest speed fluctuation amplitude among the three algorithms, demonstrating its strong robustness and stability in the presence of continuous disturbances. Fig. 2(b) illustrates the simulated torque responses of the three control methods. The results indicate that both the PI controller and NTMFSMC-SMDO scheme produce notable transient torque overshoot during speed adjustment, and considerable torque ripple persists even after reaching a steady state. In contrast, the torque generated under the ANTMFSMC-INTSMDO approach rapidly follows the reference, and its steady-state ripple is markedly diminished. When load disturbances are applied, the proposed method yields a substantially smaller torque fluctuation amplitude than the PI and NTMFSMC-SMDO strategies and shows a faster return to steady operation. These observations further confirm the enhanced ability to suppress the torque ripple and withstand time-varying disturbances. Figs. 2(c) and 2(d) present the comparative simulation results for the PI, NTMFSMC-SMDO, and ANTMFSMC-INTSMDO controllers with respect to the d- and q-axis current responses. The results show that the current ripple on both axes is considerably lower under the proposed ANTMFSMC-INTSMDO scheme than that under the PI and NTMFSMC-SMDO strategies. Even when external

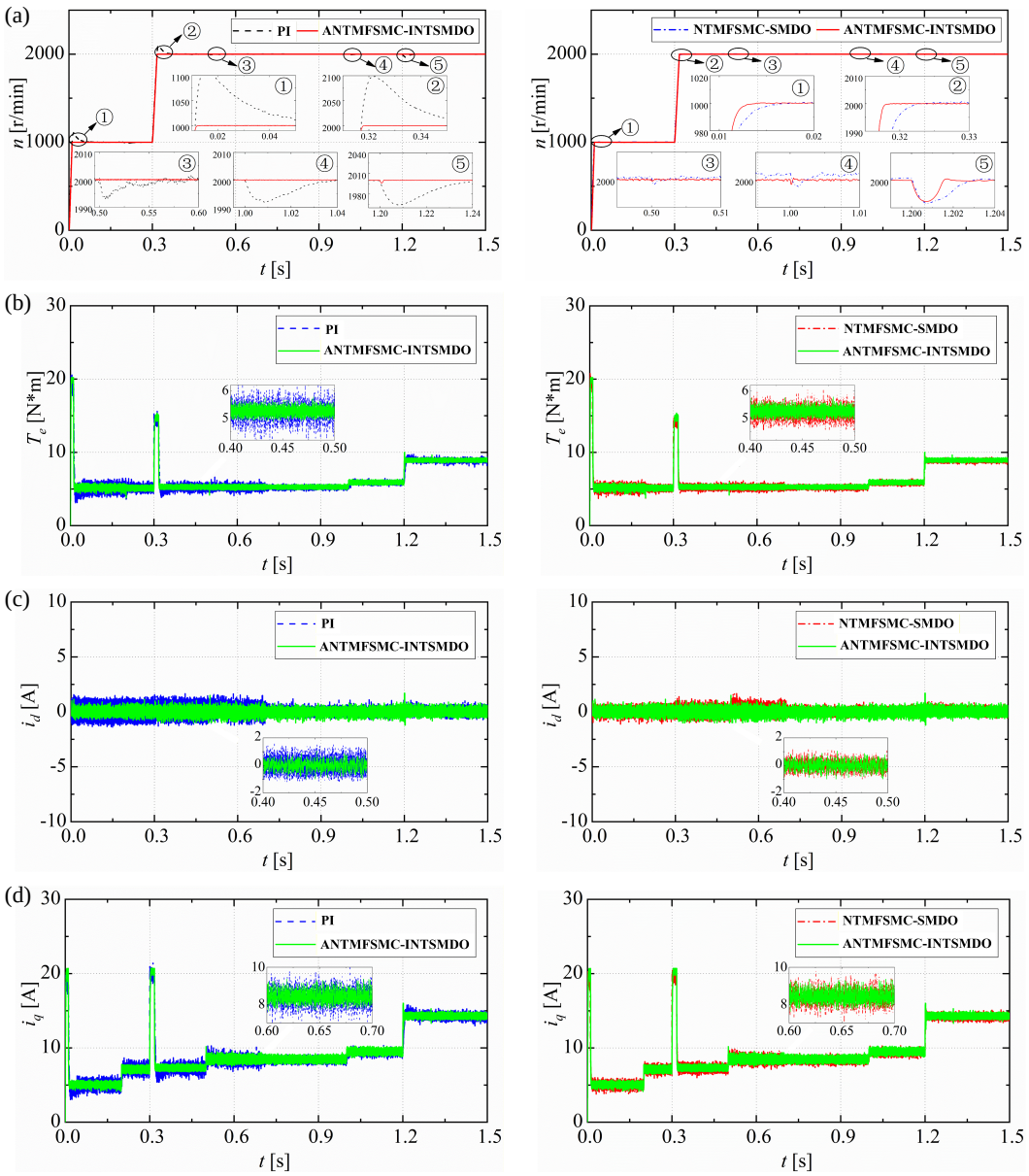

FIGURE 2. The simulation results of three algorithms. (a) Simulation results for n. (b) Simulation results for T_e. (c) Simulation results for i_d. (d) Simulation results for i_q.

disturbances are applied, the proposed method preserves the smoother d-q current trajectories, demonstrating its capability to enhance the transient and steady-state performance of the motor.

5.2. Analysis of Simulation Results of SMDO and INTSMDO

Figure 3 compares the performance of SMDO and INTSMDO. Fig. 3(a) depicts the tracking error of the three control loops, whereas Fig. 3(b) presents the corresponding disturbance estimation results. A comprehensive examination revealed that the conventional SMDO requires relatively high gains, which leads to increased tracking errors. In contrast, the INTSMDO developed in this study effectively mitigates these drawbacks, as reflected in the following observations.

i) For the speed control loop, INTSMDO yields a smoother and more accurate disturbance estimation with significantly reduced chattering, resulting in smaller speed tracking errors.

ii) In the d-q axis current loops, INTSMDO achieves faster and more precise tracking of current variations, together with improved disturbance estimation accuracy.

iii) However, SMDO demonstrates limited tracking capability and poor disturbance estimation performance, making it challenging to satisfy high-performance control demands under complex operating conditions.

Because the effectiveness of the system controller strongly depends on the accuracy of the disturbance estimation, the superior characteristics of the INTSMDO play a vital role in sup-

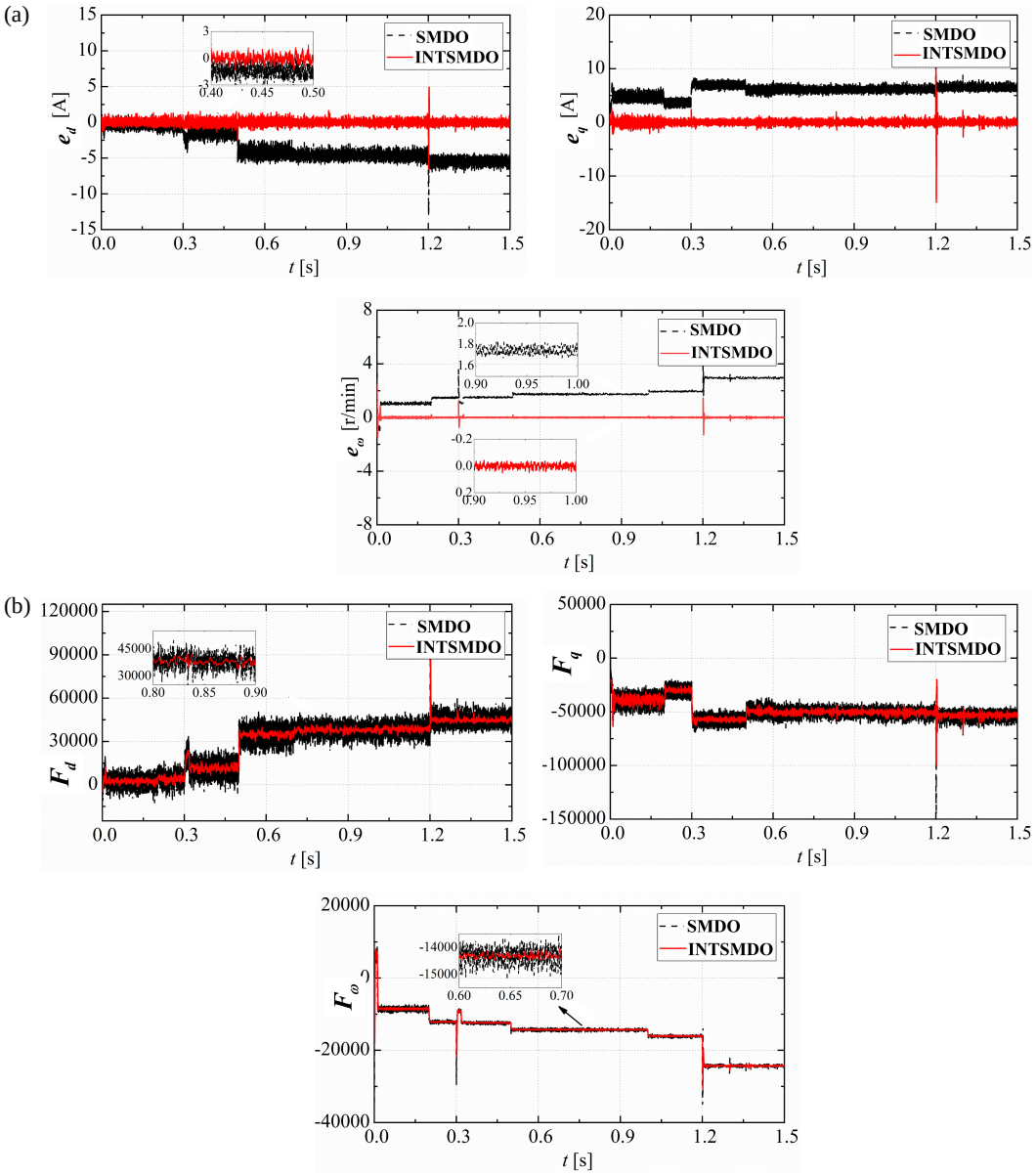

FIGURE 3. The simulation results of SMDO and INTSMDO. (a) Observed values for the tracking errors of i_d, i_q, and n. (b) Observed values of disturbance for F_d, F_q, and F_ω.

porting the proposed ANTMFSMC framework and ensuring its excellent overall control performance.

6. ANALYSIS OF EXPERIMENTAL RESULTS

To further validate the effectiveness of the proposed control strategy, hardware-in-the-loop (HIL) simulations for the PMSM were performed using an RT-LAB (OP5600) platform. The overall experimental configuration is shown in Fig. 4. The DSP (TMS320F2812) serves as the real-time control unit, executes the control algorithm, and produces the corresponding PWM signals. The OP5600 real-time simulator was employed to construct the plant model, which includes the PMSM and inverter dynamics. After completing the controller modeling and parameter adjustment in Simulink, the generated code is downloaded to the DSP, enabling real-time control of

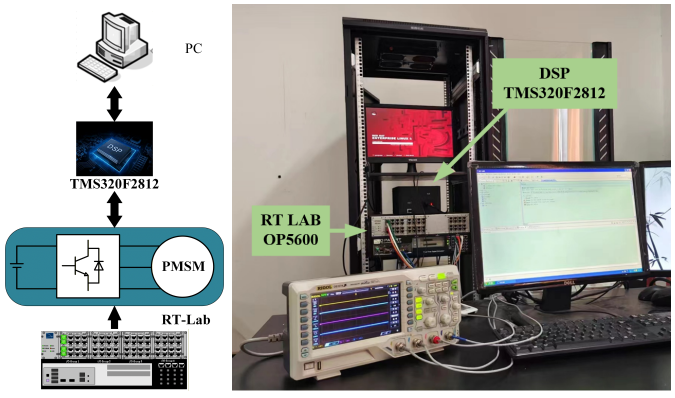

FIGURE 4. RT-Lab (OP5600) HILS experimental platform.

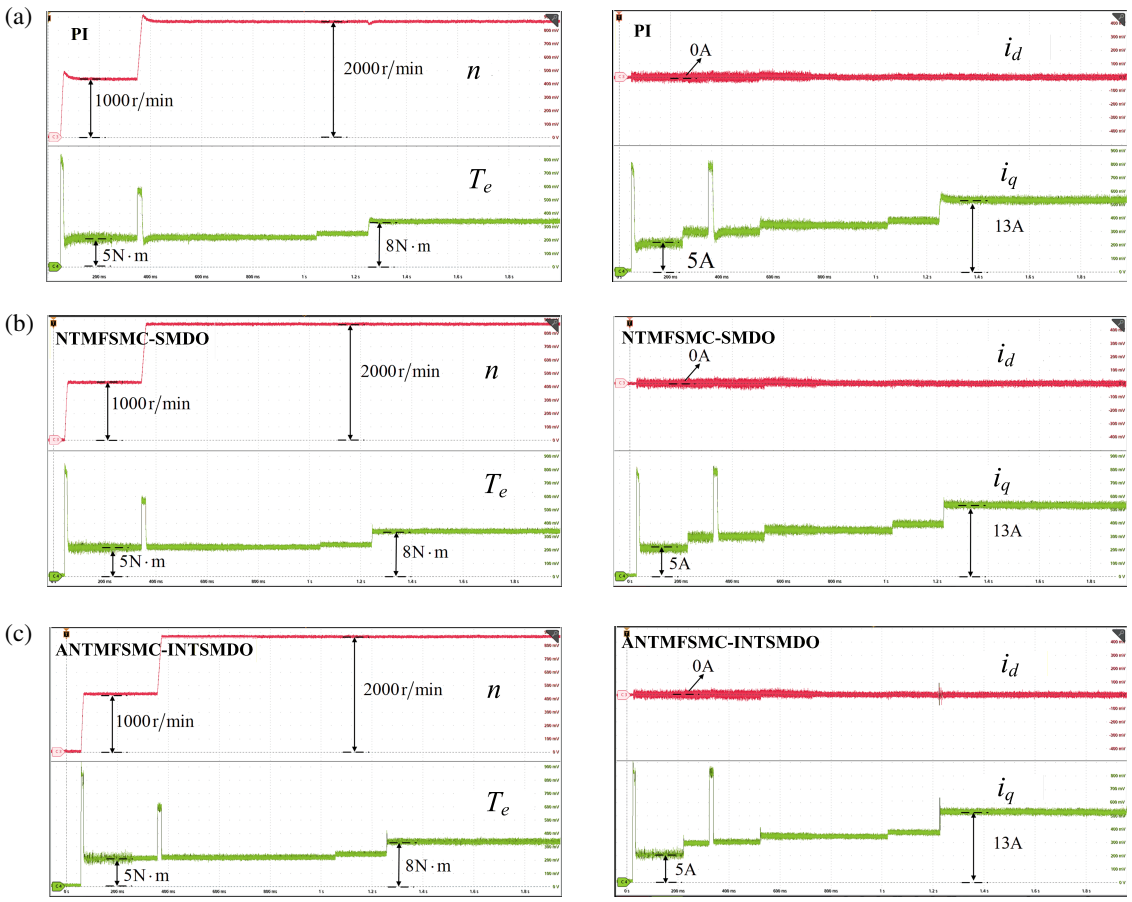

FIGURE 5. Experimental results of three algorithms. (a) Experimental results for the PI. (b) Experimental results for the NTMFSMC+SMDO. (c) Experimental results for the ANTMFSMC+INTSMDO.

the virtual PMSM system. Fig. 5 shows the experimental comparison results of the three control algorithms under full operating conditions, further validating the effectiveness and engineering applicability of the proposed strategy. The comparison schemes of the three algorithms are all run under the same settings, that is, the experimental parameter settings are consistent with the experimental conditions.

6.1. Analysis of Experimental Results for Three Algorithms

The experimental results summarized in Fig. 2–Fig. 5 clearly demonstrate that the proposed ANTMFSMC-INTSMDO controller maintains superior performance even in the presence of pronounced system uncertainties, including parameter variations and load disturbances. The incorporation of the INTSMDO enables precise estimation and timely compensation of the lumped disturbances, thereby effectively suppressing load-induced torque oscillations and mitigating d-q axis current ripple. As a consequence, the phase-current harmonic content is substantially reduced, leading to enhanced stability and smoother operation of the PMSM traction system. Furthermore, the controller exhibits remarkable resilience under time-varying disturbance conditions, consistently delivering high control accuracy without degradation. Owing to its reduced dependence on an exact motor model, the proposed strategy demonstrates strong adaptability to uncertain or variable operating environments. These findings highlight its practical value and provide meaningful insights for engineering implementation of high-performance PMSM drive systems, especially in applications demanding robust and reliable real-time control.

6.2. Analysis of the Total Harmonic Distortion for Three Algorithms

Figure 6 presents the A-phase current waveform and the corresponding total harmonic distortion (THD) obtained under steady-state operation for the three control strategies. Under complex operating conditions, the PI-based closed-loop control exhibits a pronounced harmonic content in the phase current, resulting in a THD of 11.4%. In contrast, the NTMFSMC approach employs SMDO to estimate the lumped disturbance F and introduces a compensating control action, thereby attenuating part of the harmonic components and reducing the THD to 7.1%, which reflects an improvement in system robustness. The proposed ANTMFSMC-INTSMDO scheme integrates a nonsingular terminal sliding-mode (NTSM) control law with an adaptive compensation mechanism, whereas INTSMDO provides a more accurate and smoother estimation of disturbance F. This combination markedly

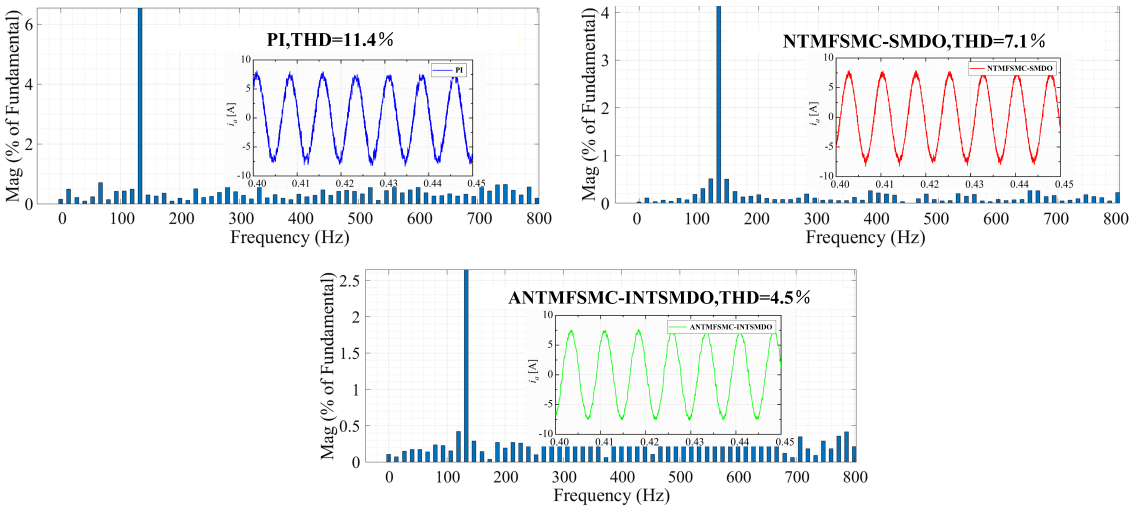

FIGURE 6. The total harmonic distortion analysis.

strengthens the disturbance rejection capability of the PMSM drive. As a result, the method not only ensures stable and reliable motor operation but also further decreases the THD to 4.5%, demonstrating a clear performance advantage over the other control strategies. Table 3 compares the overall performance of the PI control, NTMFSMC-SMDO, and the proposed ANTMFSMC+INTSMDO control strategies under load disturbance and parameter perturbation conditions. The results show that the proposed ANTMFSMC-NTSMDO method outperforms the other methods in terms of dynamic response, steady-state accuracy, and robustness.

TABLE 3. Comparison of control performance.

Performances	PI	NTMFSMC-SMDO	ANTMFSM-INTSMDO
Speed Response[1]	0.14 s	0.03 s	0.01 s
Torque Ripple	15.1%	11.2%	7.34%
THD	11.4%	7.1%	4.5%
Speed Error[2]	54 r/min	8 r/min	2.5 r/min

Note 3: 1. Speed response: the time (in seconds) required for the motor to reach a steady state after startup; 2. The magnitude (in r/min) of the speed decreased after a sudden torque change.

7. CONCLUSION

To address the limitations of PMSM speed-current closed-loop systems, including control performance degradation and insufficient convergence in traditional PI and MPCC control strategies, this study integrated model-free control with higher-order sliding mode theory to develop a novel composite control strategy. The strategy combines a model-free structure, a nonsingular terminal sliding mode algorithm, and an adaptive sliding mode reaching law to construct a control architecture in which the speed-current loop ANTMFSMC and INTSMDO observer work in coordination. In this architecture, the designed INTSMDO observer is used to accurately estimate unknown components, such as unmodeled dynamics and parameter uncertainties, present in the continuous control model of the d-q axis speed-current loop. These estimates were then introduced as feedforward compensation into the ANTMFSMC controller. Simulated and experimental results show that, compared to traditional PI control and the NTMFSMC-SMDO method, the proposed strategy effectively suppresses the ripple in the d-q axis current and voltage, significantly improving the convergence speed and disturbance rejection capability of the motor control system.

ACKNOWLEDGEMENT

This work was supported by the Postgraduate Scientific Research Innovation Project of Hunan Province Grant CX20231107.

REFERENCES

[1] Li, X., J. Liu, K. Zhao, Y. Yin, and L. Zou, "An improved model-free sliding mode control algorithm of super-twisting for SPMSM," *Progress In Electromagnetics Research C*, Vol. 135, 195–210, 2023.

[2] Lin, F.-J., S.-Y. Chen, I.-M. Hsu, and C.-X. Xu, "Robust deadbeat predict current control using intelligent integral sliding mode control for interior permanent magnet synchronous motor drive," *IEEE Transactions on Transportation Electrification*, Vol. 11, No. 3, 8282–8293, 2025.

[3] Shi, S., Y. Wang, and S. Mai, "Research on speed control of pmsm based on a new sliding mode reaching law of fast integral terminal sliding mode control with iterative-based high-gain disturbance observer," *IEEE Transactions on Industry Applications*, Vol. 61, No. 3, 4352–4363, 2025.

[4] Zhao, X. and L. Wang, "Finite-time control of permanent magnet linear synchronous motor via variable gain fractional-order terminal sliding mode control," *IEEE Transactions on Transportation Electrification*, Vol. 11, No. 4, 9105–9120, 2025.

[5] Liu, J., Z. Wang, H. Zhong, F. Deng, K. Zhao, and X. Li, "Improved active-disturbance rejection cascade control of pmsm based on new fast super-twisting non-singular terminal sliding mode control law," *Progress In Electromagnetics Research Let-*

ters, Vol. 128, 1–9, 2025.

[6] Lee, H.-W., G.-J. Nam, and K.-B. Lee, "Simple speed control strategy for a mono-inverter dual parallel permanent magnet synchronous motor drive system," *IEEE Journal of Emerging and Selected Topics in Power Electronics*, Vol. 13, No. 2, 2580–2589, 2025.

[7] Liu, J., Z. Wang, F. Deng, K. Zhao, and X. Li, "Continuous high-order sliding mode optimization control of PMSM based on STSMO," *Progress In Electromagnetics Research Letters*, Vol. 127, 29–37, 2025.

[8] Wang, S., Z. Wang, X. Niu, Y. Zhu, W. Lu, and Y. Liu, "An adaptive sliding mode control for PMSM servo systems beyond the inertia ratio limit," *IEEE Transactions on Power Electronics*, Vol. 40, No. 11, 16 352–16 366, 2025.

[9] Yu, X., X. Wu, T. Wu, D. Yang, Z. Lei, and S. Huang, "An FTSMO-based current measurement offset error compensation method in SPMSM drives," *IEEE Transactions on Industrial Electronics*, Vol. 72, No. 7, 6840–6851, 2025.

[10] Qu, L., W. Qiao, and L. Qu, "An extended-state-observer-based sliding-mode speed control for permanent-magnet synchronous motors," *IEEE Journal of Emerging and Selected Topics in Power Electronics*, Vol. 9, No. 2, 1605–1613, 2021.

[11] Yim, J., S. You, Y. Lee, and W. Kim, "Chattering attenuation disturbance observer for sliding mode control: Application to permanent magnet synchronous motors," *IEEE Transactions on Industrial Electronics*, Vol. 70, No. 5, 5161–5170, May 2023.

[12] Xu, W., A. K. Junejo, Y. Liu, and M. R. Islam, "Improved continuous fast terminal sliding mode control with extended state observer for speed regulation of PMSM drive system," *IEEE Transactions on Vehicular Technology*, Vol. 68, No. 11, 10 465–10 476, Nov. 2019.

[13] Hou, Q., S. Ding, and X. Yu, "Composite super-twisting sliding mode control design for PMSM speed regulation problem based on a novel disturbance observer," *IEEE Transactions on Energy Conversion*, Vol. 36, No. 4, 2591–2599, Dec. 2021.

[14] Liu, Y.-C., S. Laghrouche, D. Depernet, A. Djerdir, and M. Cirrincione, "Disturbance-observer-based complementary sliding-mode speed control for PMSM drives: A super-twisting sliding-mode observer-based approach," *IEEE Journal of Emerging and Selected Topics in Power Electronics*, Vol. 9, No. 5, 5416–5428, 2021.

[15] He, Y., K. Zhao, Z. Yi, and Y. Huang, "Improved terminal sliding mode control of PMSM dual-inertia system with acceleration feedback based on finite-time ESO," *Progress In Electromagnetics Research M*, Vol. 134, 21–30, 2025.

[16] Zhang, Y., M. Zhou, W. Luo, and Z. Cheng, "An adaptive learning co-evolutionary variational particle swarm optimization algorithm for parameter identification of PMSWG," *Progress In Electromagnetics Research C*, Vol. 141, 175–183, 2024.

[17] Wang, X., J. Shen, S. Sun, D. Xiao, Y. Liu, and Z. Wang, "General modeling and control of multiple three-phase PMSM drives," *IEEE Transactions on Power Electronics*, Vol. 40, No. 1, 1900–1909, 2025.